Application of seismic inversion in estimating reservoir petrophysical properties: Case study of Jay field of Niger Delta

Meludu Chukwudi Osita[1], Chukwuemeka Patrick Abbey[2, *], Adetola Sunday Oniku[1], Emele Uduma Okpogo [3], Abraham Sunu Sebastian[1], Yusuf Mamman Dabari[4]

[1]Dept. of Physics, Modibbo Adama University of Technology Yola
[2] Dept. of Petroleum Chemistry & Physics, American University of Nigeria
[3]Gemfields Nig Ltd, Lagos Nigeria.
[4] Dept. of Geology, Modibbo Adama University of Technology Yola

***** *Corresponding Author: emexabbey@gmail.com*

Abstract

The conventional approach in reservoir characterization uses an extrapolation of petrophysical properties calculated from well logs in determining the entire field volume. This technique fails to acknowledge the heterogeneity of a reservoir and consequently leads to errors (under or over-estimation) in reservoir capacity quantification. This research employs a deterministic seismic inversion approach in determining the petrophysical properties of each reservoir sand. First, the reservoir sand was identified from intervals of low gamma-ray value with corresponding high resistivity log value. Then, a synthetic seismogram was generated to tie the well to the seismic data and identify events corresponding to the reservoir sands. This was done by convolving the developed reflectivity series, derived from approximated Zeoppritz reflectivity with a zero-phase wavelet generated using the seismic. Acoustic impedance from the well and seismic were analyzed and strongly correlated. The impedance was then constrained with determined petrophysical parameters from the well, and it was used in generating the petrophysics base model used in the inversion. Finally, deterministic seismic inversion was carried out to determine the petrophysical properties such as porosity, the volume of shale, and water saturation associated with the fluids from the seismic volume of Jay-field shallow offshore of Niger Delta.

Keywords: acoustic impedance; petrophysical properties; reservoir; Seismic inversion; well logs.

1. Introduction

Exploration of hydrocarbon worldwide, especially in the frontier basin, has increased which is depends on the need to meet global hydrocarbon demands and consumption challenges. Reservoir characterization implies a geophysical methodology to quantify the reservoir potentials and facies associated with the trapped fluids in the subsurface. This goes beyond delineating the lithology's faults, traps, migration pathway for the reservoir fluids, and the determination of hydrocarbon layer depth in the ground and moveable potential fluids within the enclave structure. Over the years, many approaches have been employed in characterizing reservoir formations to quantify the amount of hydrocarbon in place and hydrocarbon recoverable.

Petrophysical properties such as rock porosity, the volume of shale within the enclave reservoir, the ratio of water saturation content, and probably the facies identification are mostly the parameters evaluated when characterizing a reservoir. These parameters describe the heterogeneity of the reservoir and are used in obtaining net-to-gross, hydrocarbon content (1-Sw), moveable hydrocarbon, and reservoir engineering simulation and recovery plan. With seismic inversion, these parameters can be determined beyond the good points in the formation. This presents a reliable estimation across the reservoir in a 2D or 3D volume for critical analysis and field development.

In recent times, geoscientists have effectively used seismic inversion as a critical tool in reservoir characterization in reducing the risk associated with oil and gas exploration and reservoir development. Adedeji (2016) explained that global optimization techniques are employed during seismic inversion to solve the problem related to hydrocarbon trapping within thin lithological beds. Seismic inversion results offer high resolvability and a better link between seismic data and lithology (Li, 2001; Sacchi & Ulrych, 1995; Adedeji, 2016).

Seismic inversion involves the estimation of wavelet from the seismic volume, the convolution of the inverse wavelet with seismic information to obtain the reflectivity, which is the transformed to interface reflection profile to get lithology profile (Li & Zhao, 2014). This suggests that the inversion process is model driven because the observed seismic data can be considered a forward model. The seismic wavelet is convolved with the earth's reflectivity series (Adedeji, 2016).

These techniques build geological models and calculate the seismic responses of the models based on known well log data. This is done by minimizing an objective function, which is usually a mismatch between the forward synthetic and the observed seismic data (Zhang *et al.,* 2012). The generated model gives critical insight into the description of the physical properties of the subsurface reservoirs. This work hopes to use the seismic and well logs available in this field to determine the petrophysical properties such as water saturation, the volume of shale, and porosity values from the seismic section by applying seismic inversion probabilistic neural network technique.

1.2 Basic Geology of the Study Area

The case study area, the Jay Field situated in the Niger Delta, is within the Gulf of Guinea on the West Coast of Africa. It is located at the southeastern end of Nigeria, bordering the Atlantic Ocean, and extends from about latitudes 400 to 600 N and longitudes 300 to 900 E. The delta was formed at the point of a rift triple junction during the opening of the southern Atlantic from the late Jurassic era, which continued into the Cretaceous (Lehnar & Ruiter, 1977). The primary deformational process in the basin continued with a downward slope of large masses of rocks under gravitational force, producing intricate folds and faults. Next was an internal deformation induced by shale mobility, and kulke (1995) explains that it occurs in two processes. First, shale diapirs were formed from the loading of poorly compacted, over-pressured prodelta and delta-slope clays (Akata

Formation) by the higher density delta-front sands, Agbada Formation, and the Second which is slope instability that proceeds due to lack of lateral, basinward support for the under-compacted delta-slope clays known as Akata Formation. As a result, the delta contains only one identified Petroleum system (Klett *et al.*, 1997, Ekweozor & Daukoru, 1994, Kulke, 1995), referred to as the Tertiary Niger Delta the Akata – Agbada petroleum system. Odebeatu & Alexander (2006) recorded that the Delta sequence is extensively affected by syn-sedimentary and post-sedimentary normal faults, which can be traced over considerable distances along with strikes. These faults are predominantly found in the Akata- Agbada formation of the delta; the remaining formation, the Benin formation, is not faulted. It comprises unconsolidated sandstones deposited in the Eocene to recent. Figure 1a is the Niger Delta province in the Gulf of Guinea with the base map of the study area, while Figure 1b is the original seismic section with the inserted well.

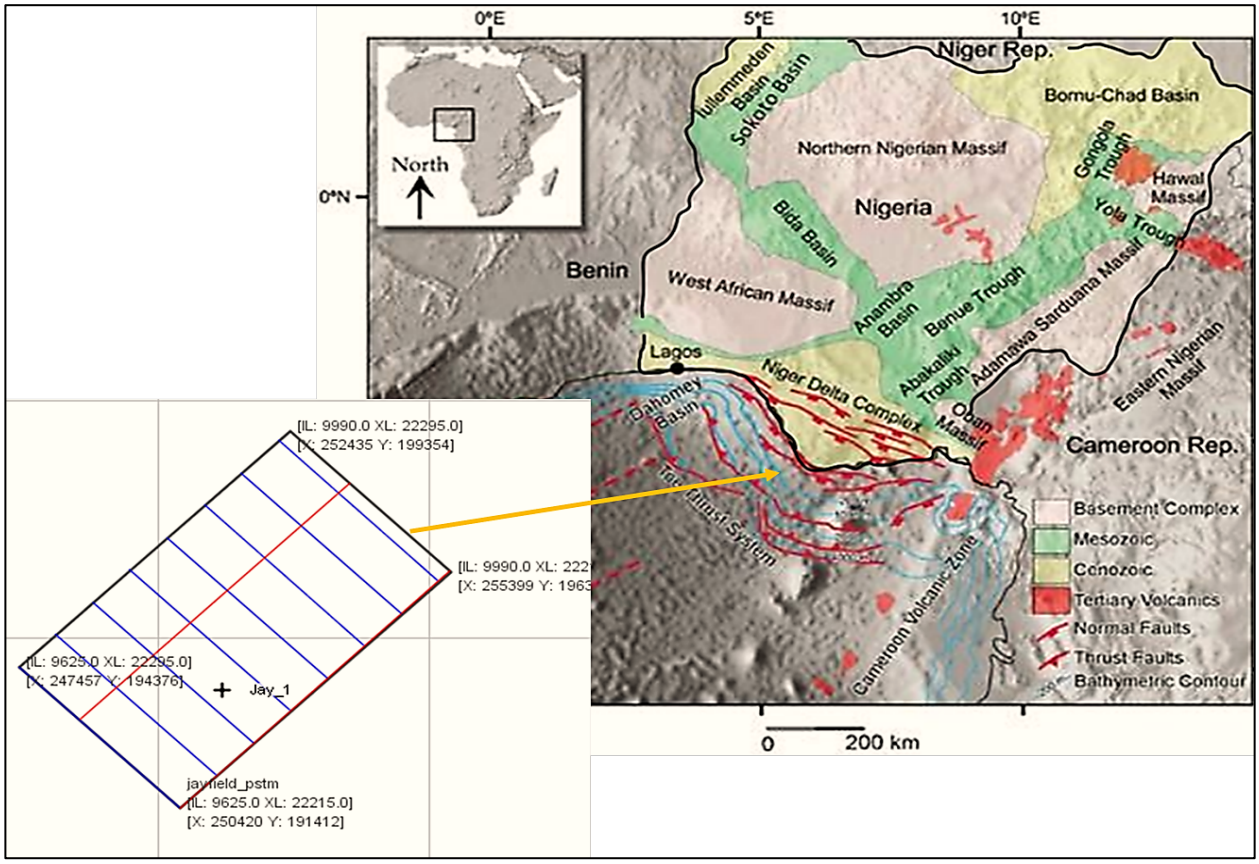

Fig. 1a. Sedimentary basin showing Niger Delta province in the Gulf of Guinea with the base map of the study area (modified from Corredor *et al.*, 2005)

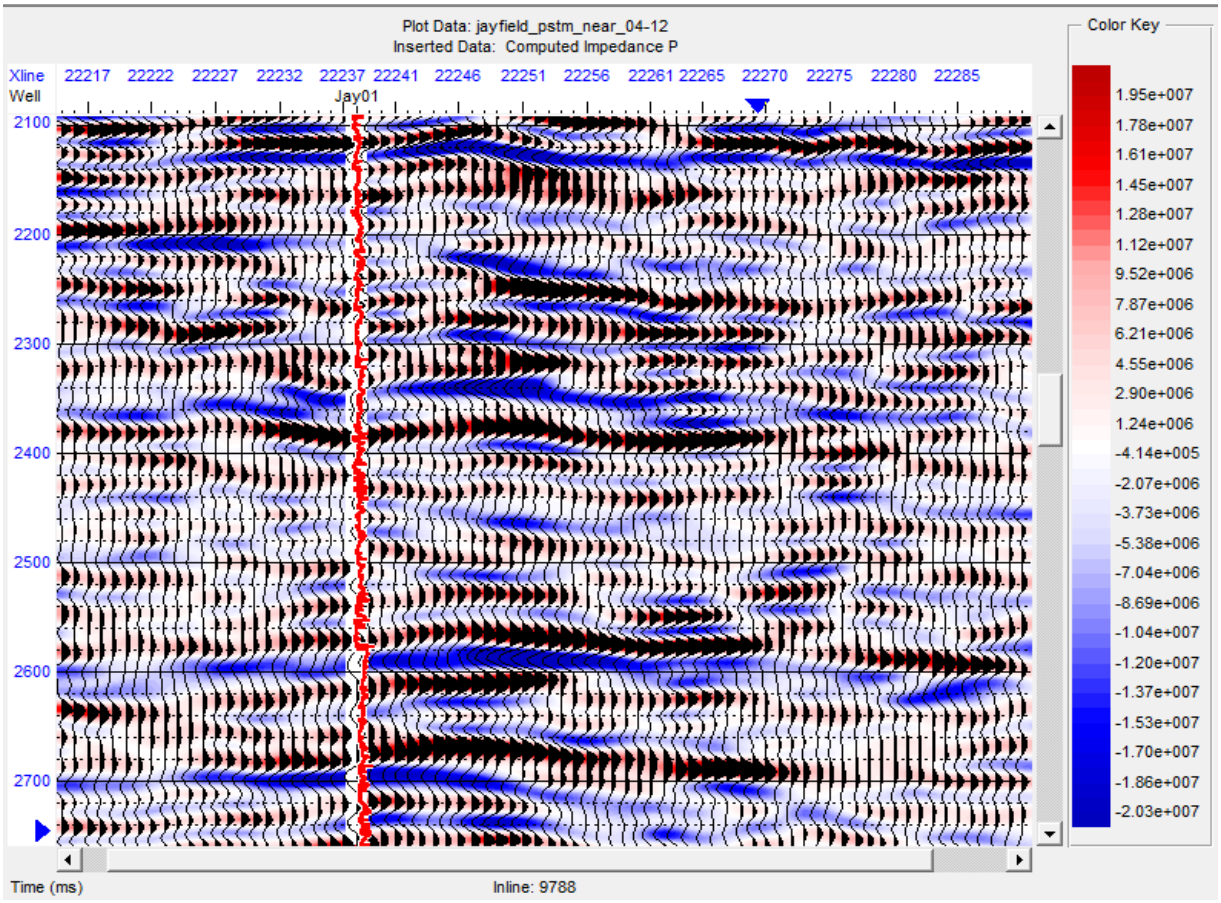

Fig. 1b. The seismic section shows the field's inserted well.

2. Materials and Method

Chevron Nigeria Limited provided the seismic and well logs data for this research through the Department of Petroleum Resources (DPR). The data comprise a 3D post-stack seismic volume and a well data that contains several well logs. The 3D survey grid and well log location are represented in Figure 1. The data were loaded into the software and were moved into a spreadsheet for quality control check (QC). The spikes noticed in the well logs were de-spiked to improve the signal-to-noise ratio. The details are as follows below with the flow chart methodology in Figure 2.

A synthetic seismogram was generated to tie the well to the seismic data and identify events corresponding to the top and base of the target events. This was done by convolving the developed reflectivity series derived from approximated Zeoppritz reflectivity equation 2.5 with a zero-phase wavelet generated using the seismic. $R = \frac{z_2 - z_1}{z_2 + z_1}$ (2.5)

Where R is the reflection coefficient, Z_1 is the acoustic impedance of the layer above, Z_2 is the acoustic impedance of the layer below in $kgm^{-2}s^{-1}$, R is unitless.

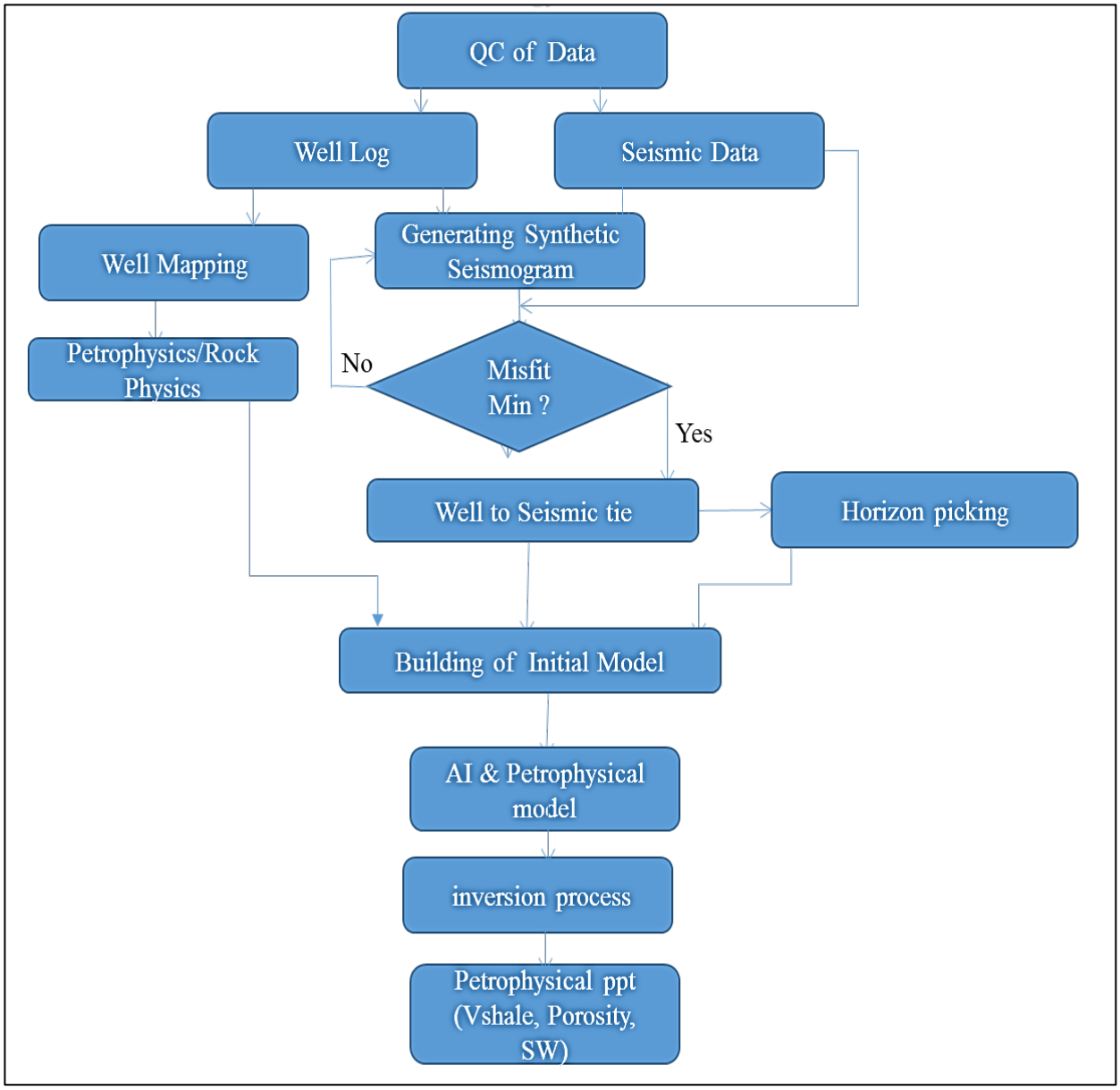

Fig. 2. Flow chart of the applied method

The deterministic forward model approach was used in the inversion process. This allows the derivation of model impedance from reflectivity and a source wavelet as in equation 2.1 from Zhang *et al.* (2012).

$$s(t) = r(t) * w(t) + n(t) \tag{2.1}$$

From the equation 2.1, $s(t)$ represents the seismic trace, $w(t)$ is the wavelet extracted, $r(t)$ is the reflectivity series, and $n(t)$ remains the random noise.

The acoustic impedance of each layer is estimated as a product of the Density and the compressional velocity traveling through the layers and is given as:

$$I_t = v_t \times \rho_t \tag{2.2}$$

Where I_t is acoustic impedance in $kgm^{-2}s^{-1}$ or $gcm^{-2}s^{-1}$

The inversion of $s(t)$ in equation 2.1, $r(t)$ will be obtained, which is the earth reflectivity series.

By, making use of $r(t)$, the layers properties are deduced because it gives interface information between geologic layers.

Since $r(t)$ is related to acoustic impedance in equation 2.3

$$r_t = \frac{I_{t+1} - I_t}{I_{t+1} + I_t} \cong \frac{\Delta I_t}{2I_t} \tag{2.3}$$

Where r_t is unit less

A non-linear statistical relationship, the probabilistic neural network (PNN), was used in establishing the connection between acoustic impedance (product of Density and velocity) and petrophysical properties (Vshale, Porosity, and Sw). This was used to transform the acoustic impedance into petrophysical properties. The process followed the defining weight factor, which is used to estimate the artificial log from the seismic traces in connection with the seismic attribute, a non-linear approach, making it easier to recognize the systematic training pattern for the prediction. The PNN derives a multi-attribute transform that non-linearly transforms the seismic attribute into well log data (Haris *et al.,* 2017). This is based on convolution operation to match the frequency of the seismic and the log data. In implementing PNN, petrophysical (SW, Porosity, and volume of shale) logs were estimated with multi attributes as training inputs.

4. Result and Discussion

Figure 3 is the schematic representation of the well logs in the well column. The first in the queue is the gamma-ray log showing the two lithologies present in the formation, the sandstones in yellow coloration and the shales in gray color. This is followed by the resistivity log, with the higher values corresponding to the yellow-colored sandstone representing the reservoir rocks (Reservoir sand A, B, C, and D). Next to the P-wave, the Density and computed acoustic impedance (product of Density and P-wave velocity). The seismic trace in blue follows the generated synthetically. The generated synthetic trace matches the trace, and it assisted in the well to seismic tie, which is used in mapping out the reservoir sands in the seismic volume. The lithology identified in the reservoirs are sandstones with shale intercalation.

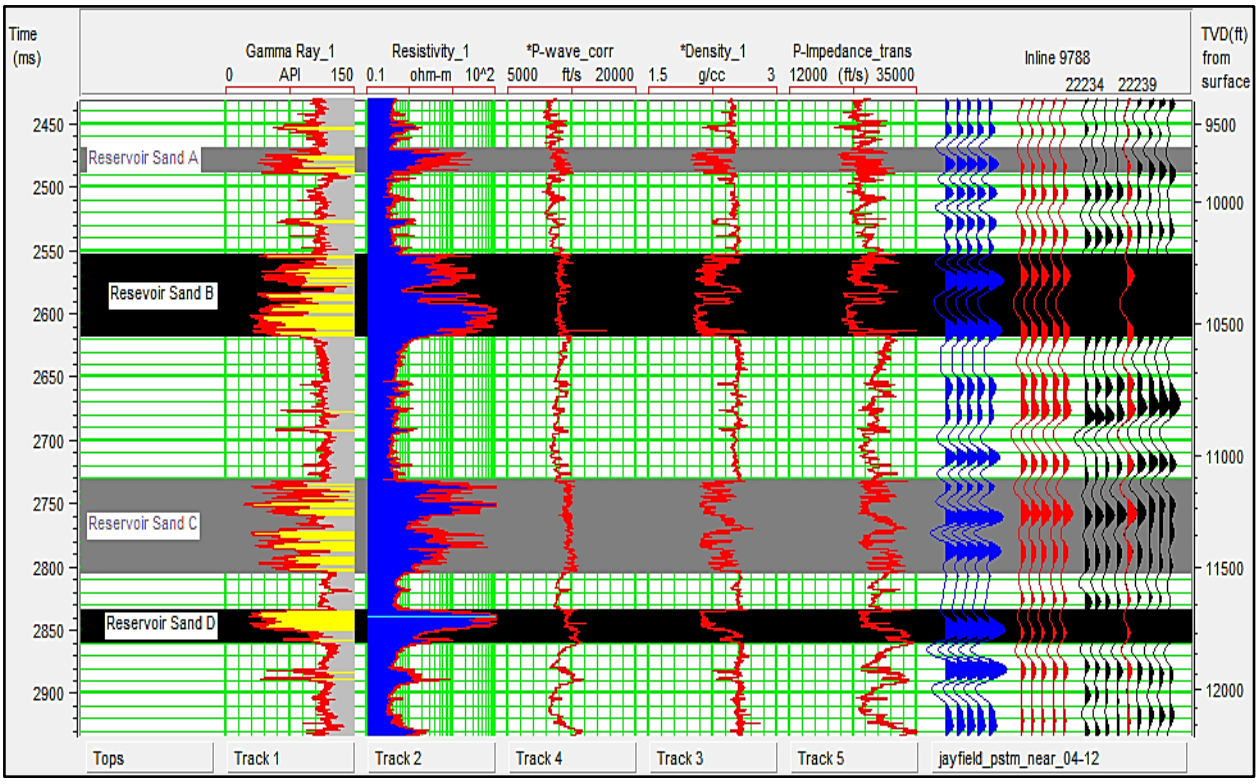

Fig. 3. Schematic of the well logs, showing the Gamma-ray log with the yellowish depict and the sandstones and the gray part the shales. Also, is the resistivity, the p-wave, Density, computed impedance logs, the synthetic (in blue), and the seismic trace (in red and black). The mapped reservoirs are sand A, B, C, and D, as shown in the diagram**.**

The inverted acoustic impedance from the seismic trace aligns with the computed impedance (shown in the well column) from the well log. The acoustic impedance result depicts gas sand as evident in the yellow rectangular box with low acoustic impedance observed in sand B reservoir. In general, across the reservoirs, the acoustic impedance increases down the formation except for the spots mentioned above. The density log and the inverted seismic Density in Figure 5 aligned with each other, revealing low Density in the reservoir sand zones. These complement the mapped reservoirs as sandstones with good to very good porosity for hydrocarbon accumulation. From the inverted section in Figure 4, reservoir sand B appears to have low-density sediments than the other identified reservoirs. This makes it the cleanest reservoir based on the verified density value, and Figure 6b complements this assertion with the minor shale content against the other reservoirs.

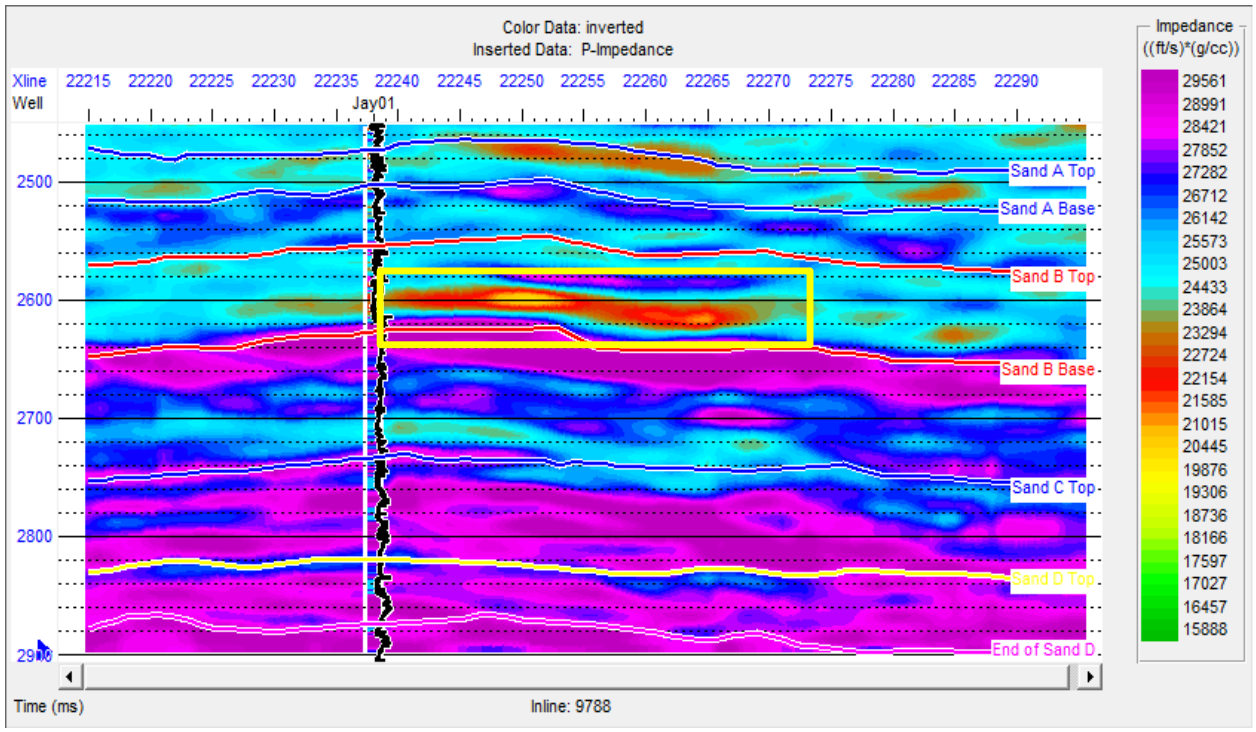

Fig. 4. Acoustic impedance generated from the seismic inversion, showing the mapped reservoir sand and low impedance reflection zones.

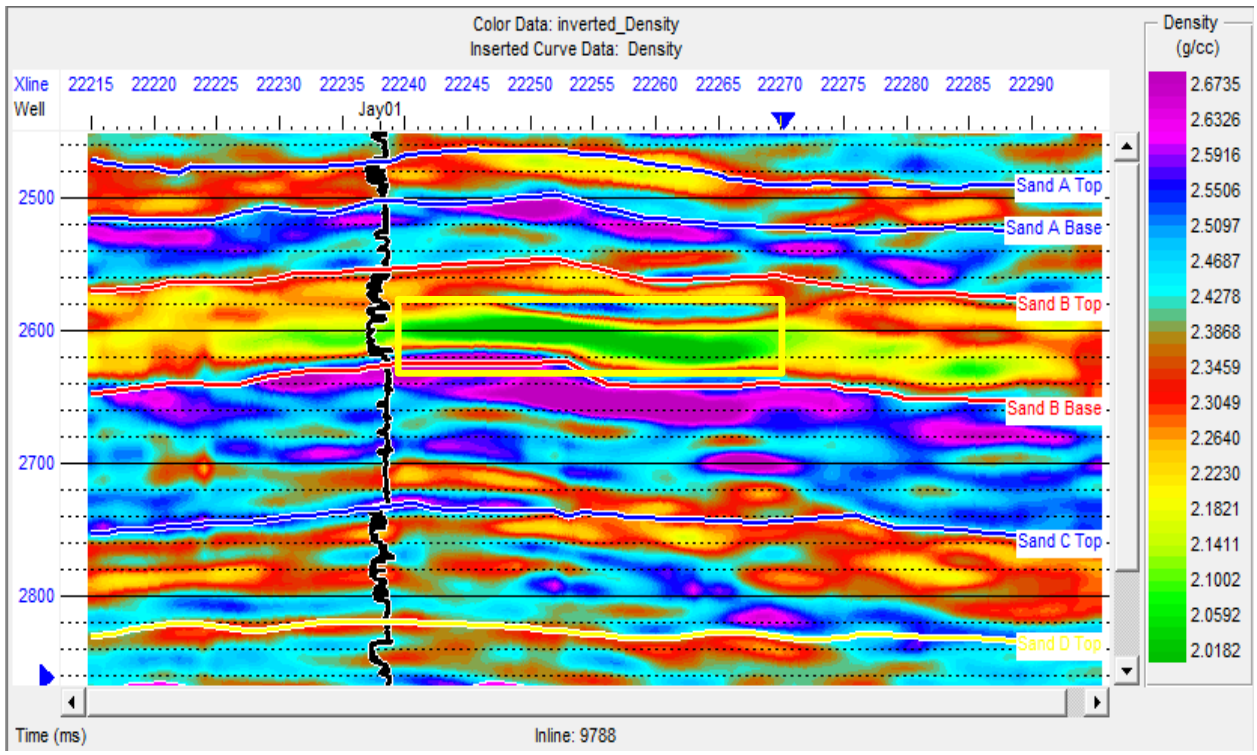

Fig. 5. Seismic inverted density section showing the inserted density log from the well. A low-density area is also revealed in the mapped reservoir sand B

The porosity, volume of shale, and water saturation of the four identified reservoirs are illustrated in Figure 6. The reservoir's productivity can be quantified via its porosity, which determines its accumulation capability. From the evaluation of the result obtained, the porosity across the entire reservoirs appears to be in the range of 0.14 to 0.24. The breakdown of the mapped reservoirs reveals that the porosity of sand A reservoir is on the average of 0.22, reservoir sand B has an average of 0.20 porosity value. In contrast, Reservoir sand C and D have porosities of 0.18 and 0.16, respectively. The obtained porosities from the seismic section complement porosity decrease with depth in a typical depositional environment. From the result obtained, reservoir sand A has the best porosity value, followed by sand B, C, and D; this implies that reservoir sand A has a better porosity range than the other reservoirs. Considering the volume of shale content and water saturation in the reservoirs, the sand B reservoir from the inverted result proves to have the least water saturation of about 48%. This shows that the hydrocarbon saturation in this reservoir stood at 52%, and the volume of shale associated with this same reservoir is about 0.36 v/v, as observed from the result. With these parameters, including the porosity of about 0.20, it can be deduced that reservoir sand B is better than the others. Reservoir sand A, C, and D have a volume of shale content of 48 v/v, 37 v/v, and 47 v/v, respectively, with a corresponding value of water saturation of about 80%, 56%, and 79%. From the mapped-out reservoirs from the well log section Figure 3, reservoirs sand C and D seem to be separated by a shale thickness of about 30 ft, which invariably should serve as a seal. However, the inverted results from seismic reveal interconnectivity of the two reservoirs C and D, suggesting linkage of the two reservoirs. This observation necessitates the mapping of sand C top without including sand C base because, presumably, sand C extends to sand D from the result obtained from the seismic inversion process.

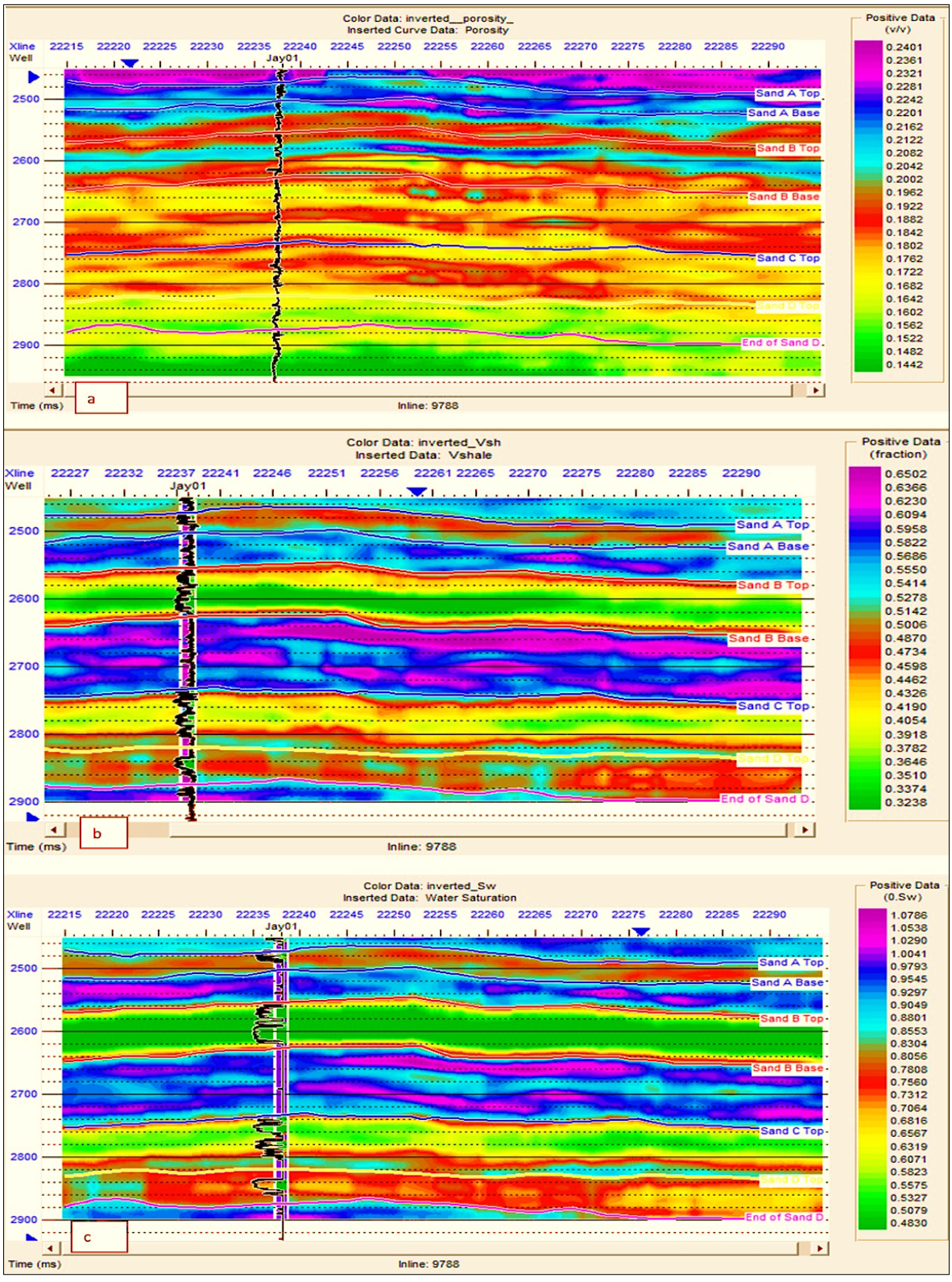

Fig. 6. a) The inverted result of the porosity from the mapped reservoirs, b) the volume of shale in the mapped reservoirs, c) water saturation estimated from the seismic section.

5. Conclusion

This research identified four reservoirs of sands of A, B, C, and D from the field using the gamma-ray, resistivity, and density logs. The estimated petrophysical quantities from the well were used to calibrate the generated acoustic impedance from the well and seismic volume. The impedance base petrophysical model was obtained, and it was inverted to create the petrophysical parameters from the seismic volume. The result showed lateral variations of porosity, the volume of shale, water saturation from the seismic section, and the quantification of these properties in the identified reservoirs. When viewed in 3D, the obtained results give clear insight for secondary recovery and justify the need for infill wells to improve production capacity.

Reference

Adedeji, E. A. (2016). 3D Post-Stack Seismic Inversion using Global Optimization Techniques: Gulf of Mexico Example. *University of New Orleans Theses and Dissertations*. 2231. https://scholarworks.uno.edu/td/2231

Haris, A. Sitorus, R. J and Riyanto, A (2017). In Proceeding Southeast Asian Conference on Geophysics, Bali, 2016 (IOP Conference Series: Earth and Environmental Science,) Vol. 62, pp. 012021.

Corredor, F., Shaw, J. H, Bilotti, F. (2005). Structural styles in the deep-water fold and thrust belts of the Niger Delta AAPG Bulletin **89** (6): 753–780. DOI.org/10.1306/02170504074

Ekweozor, C. M. & Daukoru, E.M. (1994). Petroleum Source Bed Evaluation of Tertiary Niger Delta--reply: American Association of Petroleum Geologists Bulletin, **68**: 390-394.

Klett, T. R., Ahlbrandt, T. S., Schmoker, J. W. and Dolton, J. L. (1997). Ranking of the World's Oil and Gas Provinces by Known Petroleum Volumes: *U.S Geological Survey Open-file Report.* 97 – 463

Kulke, H. (1995). Nigeria Regional Petroleum Geology of the World Part II (Eds. Kulke, H): Africa, America, Australia and Antarctica: Berlin, Gebruder Borntraeger, **11**:143-172.

Lehnar, P. and De Ruiter, P.A. (1977). Structural History of Atlantic Margin of Africa AAPG Bulletin, **16**: 961 –981.

Li, Q. (2001), LP sparse spike inversion, Strata Technique Document, Hampson-Russell Software Services Ltd.

Li, M, and Zhao, Y. (2014). Geophysical Exploration Technology - Applications in Lithological and Stratigraphic Reservoirs, Chapter 6 - Seismic Inversion Techniques, 2014, Pages 133-198, https://doi.org/10.1016/B978-0-12-410436-5.00006-X

Odebeatu, A. & Alexander, G. (2006). Application of Spectral Decomposition to Detection of Dispersion Anomalies Associated with Gas Saturation, The Leading Edge, (25): 205-210

Sacchi, M. D. & Ulrych, T. J. (1995). High-resolution velocity gathers and offset spacereconstruction: Geophysics, 60, 1169-1177.

Zhang, R., Sen, M., Phan, S., & Srinivasan, S. (2012). Stochastic and deterministic seismic inversion methods for thin-bed resolution, *J. Geophys. Eng*. 9 (2012) 611–618 doi:10.1088/1742-2132/9/5/611.

Submitted: 20/11/2020
Revised: 21/05/2021
Accepted: 15/06/2021
DOI: 10.48129/kjs.10229